Selective silencing rather than targeted activation of gene expression underlies fate choice in human hematopoietic stem cells

Parmentier R[1]*, Moussy A[1]*, Chantalat S[2]*, Racine L[1], Sudharshan R[3,4], Papili Gao N[4], Stockholm D[1], Corre G[5], Deleuze JF[2], Gunawan R[3], Paldi A[1].

[1] Ecole Pratique des Hautes Etudes, PSL Research University, St-Antoine Research Center, Inserm U938, 34 rue Crozatier, 75012, Paris, France

[2] Centre National de Recherche en Génomique Humaine, CEA, 91000 Evry, France

[3] Department of Chemical and Biological Engineering, University, Buffalo, NY 14260, USA

[4] Institute for Chemical and Bioengineering, ETH Zurich, 8093 Zurich, Switzerland

[5] Genethon; 1bis rue de l'International, 91001 Evry, France

* Equal contribution

Abstract:

When human cord blood derived CD34+ cells are induced to differentiate *in vitro*, they undergo rapid and dynamic morphological and molecular transformation that are critical for the fate

commitment. Using ATAC-seq and single-cell RNA sequencing, we detected two phases of this process. In the first phase, we observed that a rapid and widespread chromatin opening - that makes most of the gene promoters in the genome accessible - precedes a global upregulation of gene transcription and a concomitant increase in the cell-to-cell variability of gene expression. The second phase is marked by a slow chromatin closure that precedes an overall downregulation of gene transcription and the emergence of coherent expression profiles that characterize distinct cell subpopulations. We further showed that the accessibility of promoters has a crucial effect on whether transcription factor changes will lead to alterations in the expression of their target genes. Our observations are consistent with a model based on the spontaneous probabilistic organization of the cellular process of fate commitment.

Background

Hematopoietic cells are a widely used model for the study of fate decision and cell differentiation and it is frequently considered as a paradigm of cell differentiation in general. Differentiation is believed to proceed through a series of binary fate decisions under the action of key instructive factors inducing specific changes in the cell that lead to stepwise switches of the expression profiles at critical decision points [1]. The typical representation of this process is a hierarchical decision tree. Such a strict hierarchical process must imply tight regulation of gene expression. The genes involved in the process are well known [2]. But recent single-cell gene expression studies directly contradict the assumption of precise regulation and strictly ordered process. It has been shown that, soon after their stimulation for differentiation, multipotent CD34+ cells go through a phase of disordered gene expression called "multilineage primed" phase characterized by concomitant expression of genes typical for alternative lineages [3–6]. Other

46 studies demonstrated that hematopoietic stem cells (HSC) gradually acquire lineage characteristics
47 along multiple directions without passing through discrete hierarchically organized progenitor
48 populations [7]. Instead, unilineage-restricted cells emerge directly from a continuum of low-
49 primed undifferentiated hematopoietic stem and progenitor cells [7]. This phase is accompanied
50 by instabilities and fluctuation of the cell transcriptome, morphology and dynamic cell behavior
51 [6,8]. How this quasi-random gene expression pattern is generated, how it is transformed into a
52 defined gene expression profile remains unknown. In order to answer these questions, we
53 determined the order and the timescale of the early chromatin and transcriptional changes that
54 follow the induction of differentiation in CD34+ cells.
55
56 To do this, we performed single cell RNA sequencing of human cord blood CD34+ cells at
57 different time points during the 96h period following their stimulation, a period shown to be
58 critical for cell fate decision [6]. The gene expression profiles were correlated to the DNA
59 accessibility changes determined by ATAC-seq at defined time-points during the same period. The
60 experimental strategy is shown in **Fig. 1A**. The data revealed strikingly different dynamics of
61 chromatin accessibility and gene expression that challenges the classical model based on specific
62 stepwise switches.
63

64 **Keywords**

65

66 hematopoietic stem cell, fate commitment, single-cell, chromatin remodeling, ATAC-seq,
67 scRNA-seq, transcription factor, promoter accessibility, CD34+
68

Results

Single-cell gene expression analysis using RNA-seq

Human CD34+ cells were isolated from the cord blood of two healthy donors and cultured in the presence of early acting cytokines as described [6]. To identify the transcriptional signatures and estimate their variability at the earliest stages of the differentiation process, we adapted MARS-seq protocol (massively parallel single-cell RNA-sequencing, see Methods) on CD34+ cells randomly sorted at different time points (5h, 24h, 48h, 72h and 96h) after the cells were cultured in the presence of cytokines [9] . A uniform random sampling of a heterogenous population allowed us to evaluate the global changes without any preconceived ideas on the cell categories present in the population. The quantification of gene expression was calibrated using unique molecular identifier (UMI) marked RNAs. Details about quality control of the results are shown in **Additional Table 1.** In order to avoid the potential bias due to batch correction, the results of the two donors were analyzed separately.

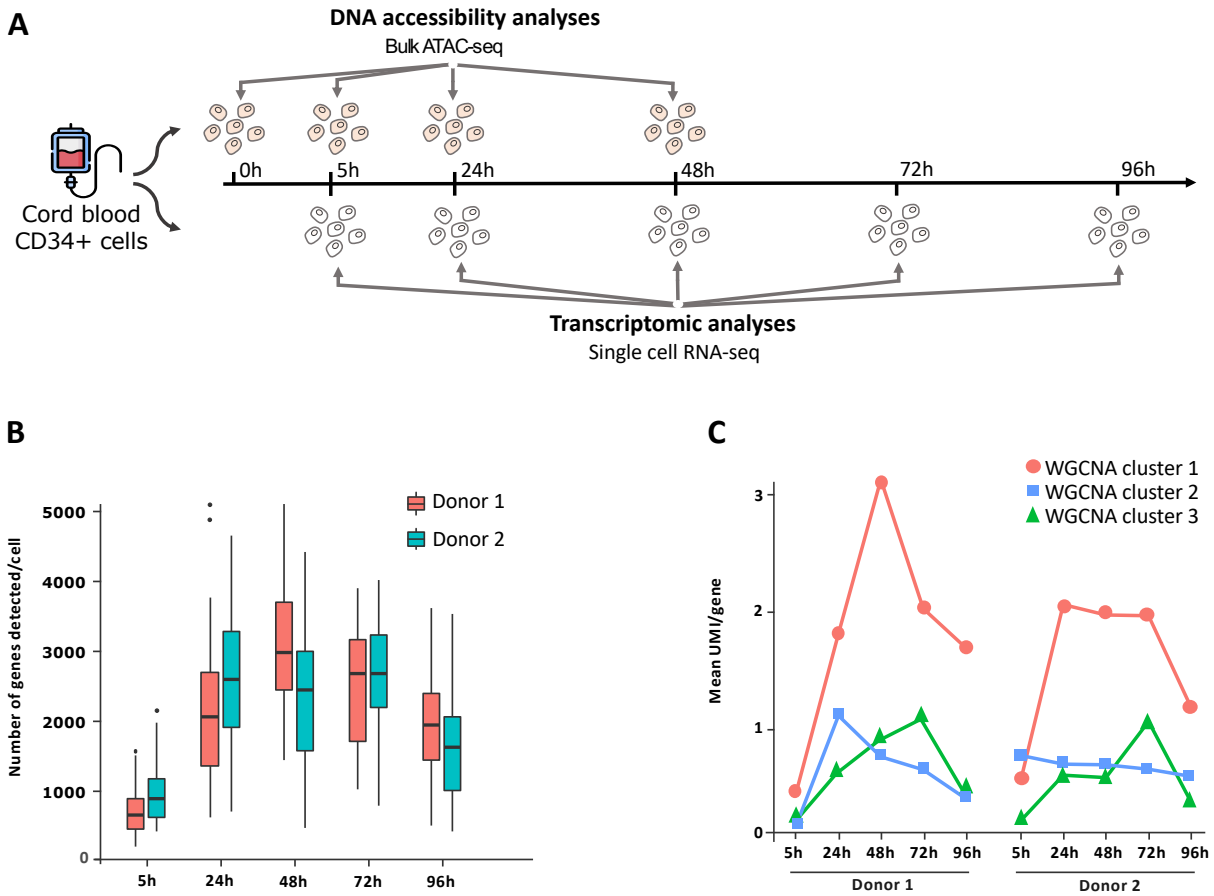

Fig. 1 Gene expression dynamics of cord blood derived CD34+ cells. A CD34+ cells were isolated from human cord blood and cultured in serum-free medium with early acting cytokines. Single-cell RNA sequencing (scRNA-seq) was used to analyze single-cell transcription at 5h, 24h, 48h, 72h and 96h. Concomitantly, at 0h, 5h, 24h and 48h, 5000 living cells were collected to perform ATAC-seq protocol in order to study DNA accessibility dynamics. **B** Number of detected genes per cell with scRNA-seq. Two donors were analyzed separately, both showed similar dynamics. **C** Weighted correlation network analysis (WGCNA) reveals clusters of genes with similar dynamic patterns in the average mRNA expression in Donor1 and Donor2. Note that cluster 1 reproduces the dynamic pattern observed for genes showing detectable expression in single cell in **Fig. 1B**. Cluster 1 = 5194 genes (Donor1) and 5518 genes (Donor2), cluster 2 = 3977 genes (Donor1) and 2602 (Donor2), cluster 3 = 1089 genes (Donor1) and 609 genes (Donor2).

97

98 The results revealed important features of the gene expression dynamics (**Fig. 1**). Following
99 stimulation, the transcriptome of the cells underwent rapid and substantial quantitative and
100 qualitative changes. Both the number of expressed genes per cell and the number of mRNA
101 molecules per gene increased substantially (**Fig. 1B and Fig. 1C**). The average number of genes
102 detected per cell at 5h was only 512+/-243 in Donor1. This number increased to 1693 +/-813 at
103 24h and 2543+/-751 at 48h, but then decreased to 2014+/-714 at 72h and to 1612 +/-613 at 96h.
104 The numbers for the cells from Donor 2 were very similar (**Fig. 1C**). The rapid increase of global
105 transcription activity in the cells, that occurred mainly during the first 48h, suggests that cells
106 significantly expand their repertoire of transcribed genes during the initial period of differentiation.
107

108 When individual genes were examined, we observed that the corresponding number of mRNA
109 molecules also increased. Using Weighted Correlation Network Analysis (WGCNA), we found
110 clusters of genes with highly correlated mean expression patterns over time (**Fig. 1C**). The three
111 largest clusters together contain more than 8500 genes with mean expressions that generally show
112 a characteristic time profile with an initial increase followed by a subsequent decrease. Thus, the
113 average CD34+ cell responds to cytokine stimulation by a strong, but transitory, upregulation of
114 transcriptional activity both in terms of the number of genes and the number of transcripts. Due
115 to the very high number of genes in the first cluster, gene ontology (GO) analysis was
116 unsurprisingly irrelevant and showed significant enrichments for all basic cellular functions.
117 Notably, none of the most represented functions were directly related to the hematopoietic lineage
118 (**Additional File. 1**). During the 24h to 48h period after the stimulation, the fraction of the genes
119 transcribed in individual cells raised up to approximately 10-15% of all genes in the genome (**Fig.**

120 **1B**). After 72h, this number started to decrease (Fig.1B). Importantly, this timing coincides with
121 the period when the first signs of lineage-specific transcriptional changes appear [6].
122
123 In order to better characterize cell type specific gene expression patterns, lineage progression, and
124 trajectory of the cells during the fate decision process, we applied a recent method CALISTA
125 (Clustering And Lineage Inference in Single-Cell Transcriptional Analysis) to the single-cell RNA
126 dataset [10]. CALISTA is a likelihood-based method that uses the two-state stochastic model of
127 gene transcription to describe the cell-to-cell variability of gene expression at single-cell level [11].
128 Here, we employed CALISTA for cell clustering, lineage inference, and calculating single-cell
129 transcriptional uncertainty. In CALISTA, to each cell is assigned a likelihood value, which reflects
130 the joint probability of its gene expression (mRNA counts) based on the mRNA distribution from
131 the two-states model. In order to avoid potential batch effects, we analyzed the single-cell mRNA
132 datasets from two donors independently. For both donors, CALISTA identified five single-cell
133 clusters on the basis of the 200 most variable genes (**Additional Fig. 1** and **Fig. 2A**). In both
134 donors, clusters #1 and #2 were essentially composed of cells isolated at 5h and 24h, respectively
135 (**Additional Fig. 2**). Clusters #3, #4 and #5 contained cells isolated at 48h, 72h and 96h, but with
136 a higher degree of cells from different time points compared to clusters #1 and #2 (**Additional**
137 **Fig. 1**). CALISTA generated the lineage progression using the clusters based on the distances
138 between each pair of clusters, specifically by adding "transition" edges in the order of increasing
139 distances and cluster pseudotimes – defined by the mode of the sampling time points of the cells
140 in each cluster. The cluster distance between any two clusters gives a measure of dissimilarity in
141 their gene expression distributions and is defined as the maximum difference in the cumulative
142 likelihood values upon reassigning the cells from the original cluster to the other cluster [10]. The

143 inferred lineage progression graphs for each of the two donors are depicted in **Fig. 2**, showing the
144 emergence of two distinct cell clusters with divergent transcription profiles.
145
146 Note that each gene in each individual cell in a cluster can be characterized by a unique likelihood
147 value (see Methods). Here, we use the negative logarithm of the gene likelihood value (NLL) as a
148 metric of transcriptional uncertainty, using which we can probe into the intra-cluster cell-to-cell
149 heterogeneity in the gene expression [10,12]. As shown in **Fig. 2B**, the gene-wise NLLs in the
150 clusters reveal that clusters #2 and #3 are much more heterogenous than the other clusters.
151 Importantly, clusters #2 and #3 contain the cells that display the highest number of expressed
152 genes and of transcripts per gene. In other words, the upregulation of global transcriptional activity
153 in response to cytokine stimulation also causes an increase in transcriptional uncertainty and cell-
154 to-cell heterogeneity in gene expression. Also, the peak of such transcriptional uncertainty
155 precedes the emergence of two distinct gene expression profiles. At 72h and 96h, both the total
156 number of transcribed genes and the number of transcripts per individual gene decrease
157 simultaneously. In a previous study, the gradual emergence of defined expression profiles was
158 observed after 72 hours [6], in agreement with our observations. The analysis of single-cell RNA
159 profiles using CALISTA above demonstrated that starting from 48h, two distinct gene expression
160 profiles start to diverge (**Fig. 2A**).
161

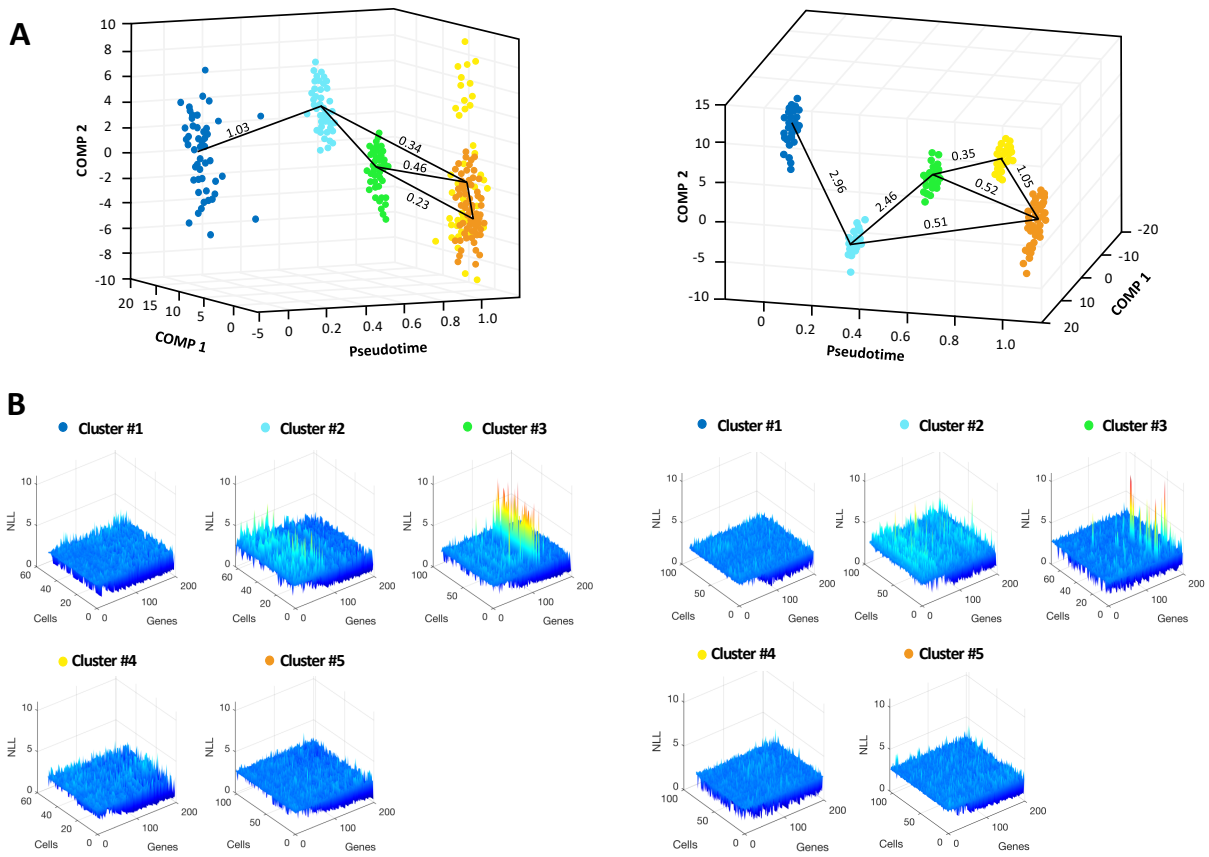

Fig. 2 Evolution of transcriptome profiles after cell stimulation. A Transcriptome clusters identified by CALISTA [10]. Each dot corresponds to a cell in the single-cell transcriptomic dataset of cells sampled at 5h, 24h, 48h, 72h and 96h. The x axis corresponds to the pseudotime values and the y-z axes to the first and second principal component (PC) coordinates. The color code for the clusters appears in Fig.2B. The transition edges are represented by black plain lines between the clusters and the numbers are "cluster distances", a likelihood-based measure of dissimilarity (distance) between cell clusters. **Left panel:** Donor1, **right panel:** Donor2. **B** Negative Likelihood matrix for the 200 most variable genes computed by CALISTA for each cluster. Each plot corresponds to a cluster indicated by a color code as in **A** and the cluster number. **Left panel:** Donor1, **right panel:** Donor2.

174 The conclusions drawn on the basis of the general trends in single-cell gene expressions are
175 supported by the expression of genes coding for transcription factors (TFs) essential for
176 hematopoietic differentiation (**Additional Fig. 2**) [2]. Notably, TF-encoding genes showed highly
177 dynamic expression by cells during differentiation. Both the fraction of expressing cells and the
178 number of mRNAs per cell increased and went through a plateau at 48-72h. However, each
179 individual cell expressed a different combination of these genes and no obvious dynamic patterns
180 could be identified. The tendency toward defined hematopoietic transcription profiles can hardly
181 be observed by the end of the time series at 96h.
182
183 In order to reveal potentially active regulatory interactions, we identified genes coding for
184 transcription factors (TFs) that showed a change in expression (**Fig. 3**). We used the terminology
185 "change" or "differentially expressed (DE)" to refer to genes that show a statistically significant
186 increase or decrease in the corresponding mRNA level based on the number of UMIs detected in
187 a cell (two-tailed Fisher exact test, see Methods for details). For each TF, we identified its target
188 genes using human transcriptional regulatory networks from the Regulatory Circuits resource [13].
189 A TF may have multiple target genes, and vice versa, a gene may have several TF regulators. A
190 gene is counted in the "changes in TF" group when at least one of the genes coding for a TF
191 targeting it shows differential expression between 5h and 24h or between 24h and 48h. Note that
192 the genes belonging to this group may or may not themselves be differentially expressed. A gene
193 is counted in the "no change in TF" group when none of its TFs show any differential expression.
194 Genes in the "changes in TF" group between 5h and 24h are significantly over-represented
195 (p=1.4e-6) for genes that are differentially expressed (i.e. DE genes), but not for those between
196 24h and 48h (**Fig. 3**). Genes in the "no change TF" group between 5h and 24h are enriched for
197 genes showing no significant differential expression, but again not for those between 24h and 48h.

198 These observations indicate that differential expression of genes between 5h and 24h is connected
199 to changes in the expression of the TF regulators, which reflects the regulatory activity of TFs.
200 However, the regulatory activity of TFs appears to have been restricted after 24h.
201

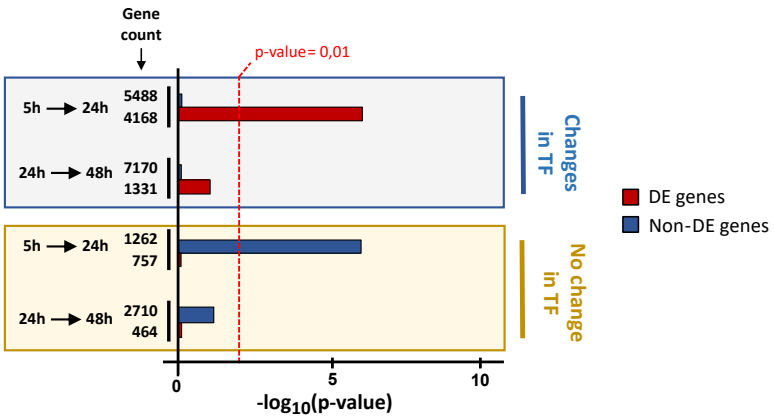

202

203 **Fig. 3 Global influence of transcription factors on targeted gene expression.** Enrichment
204 analysis of genes in the "change in TF" and "no change in TF" group for differentially expressed
205 (DE) and non-DE genes.
206

207 ATAC-seq analysis of DNA accessibility

208

209 DNA accessibility in CD34+ cells was determined using ATAC-seq [14] at four time points (0h,
210 5h, 24h, and 48h after cell stimulation). We applied a stringent filter to identify accessibility by only
211 retaining peaks that are uniformly detected in the cells of three different donors (see **Additional**
212 **Table. 2** for donor-related information). Performing ATAC-seq on 5000 cells ensured that the
213 detected accessible DNA regions are present in a substantial fraction of cells. Indeed, accessible
214 sites present in individual or a small number of cells could not be differentiated from the technical
215 noise.

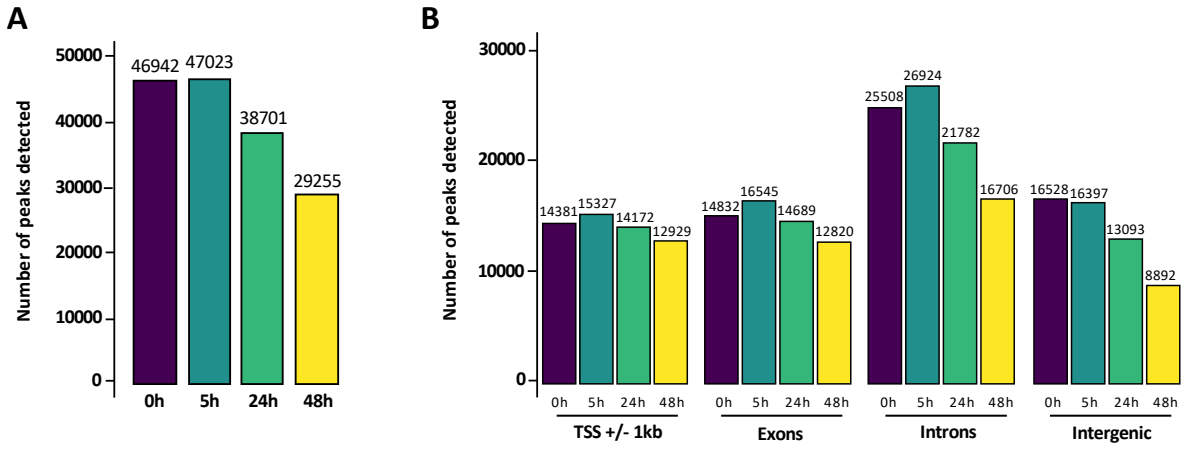

Fig. 4 Chromatin accessibility dynamics as detected by ATAC-seq. A Number of accessible regions (peaks) at 4 different time points. **B** Number of peaks in different genomic elements. A single peak may count for two categories if overlapping both. Intergenic category was defined as the exclusion of any other category tested.

Apart from the peaks in intergenic regions, the total number of ATAC-seq peaks first increased rapidly by 10-12% between 0h and 5h in all genomic regions, then decreased gradually at slower rate over the next 48h (**Fig. 4B**). The time-dependent decrease in the number of ATAC-seq peaks varied with their genomic location (**Fig. 4B**). While the number of peaks in distal intergenic regions was halved between 5h and 48h, the decrease in the other locations was less significant (**Fig. 4B**). Particularly, the number of peaks in promoter regions only dropped by 15% between 0h and 48h.

In order to further characterize the dynamics of the ATAC-seq, we also estimated the changes in the size of the peaks present at least at two consecutive time points. As a proxy for the size of a peak, we used the number of sequenced reads that define it. Here we assumed that the normalized number of reads can be used as a rough estimation of the fraction of the cells with at least one of the two copies of the region having accessible DNA. The difference of read counts for the same

ATAC peak detected at two consecutive time points was used to assess the chromatin dynamics. We calculated the log-fold changes of the number of reads of each peak for time intervals and the associated p-values and represented them as volcano plots (**Fig. 5**). We observed a significative tendency of the peaks already present at 0h to increase in accessibility by 5h (**Fig. 5**), especially for peaks located in the TSS regions. During this period, a total of 17% (9045 out of 53797 peaks) showed significant changes regarding accessibility. In the same range, between 5h and 24h, 15% (7505 out of 50936 peaks) of the peaks present at both time points changed significantly with an approximately equivalent number of increased and decreased ATAC-seq read counts. However, between 24h and 48h, only 2% (48 out of 40248 peaks) of the peaks showed differential read counts, but again, with roughly equal proportions of increased and decreased peaks (**Fig. 5**). Overall, most of the changes occurred during the first 24 hours (**Fig. 5**). First, we observed a rapid increase in peak number and an increase in size (read counts) for the peaks already present. Then the trend was reversed: both the number and size of the peaks decreased between 5h and 24h. This trend was maintained, albeit at a lesser degree, between 24h and 48h. Overall, the ATAC-seq observations indicate an unusually strong wave of chromatin fluctuations during the initial 48 hours long period. The dynamic fluctuations appear to be higher in intergenic regions than in gene-associated regions.

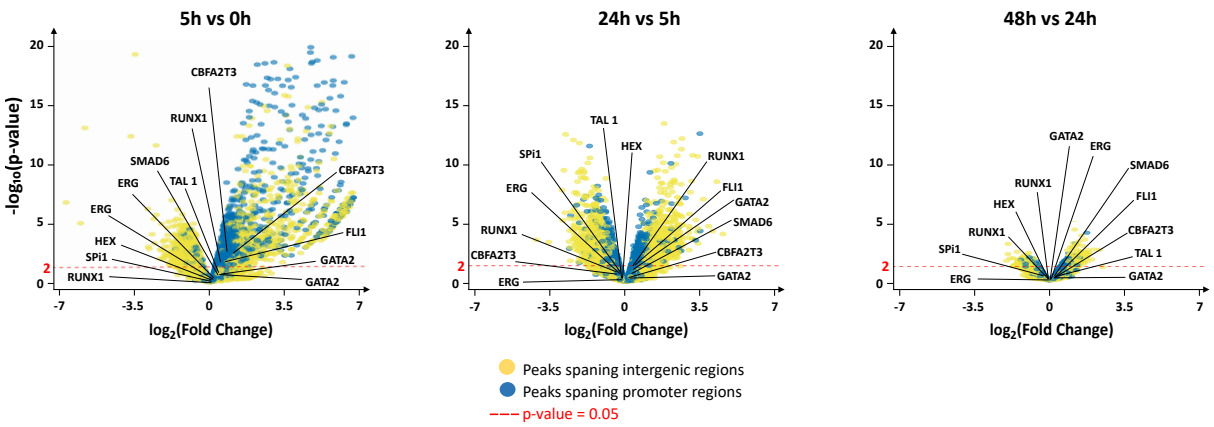

253 **Fig 5. Differential analysis of ATAC-seq peaks present at least in two consecutive time**
254 **points**. The differential analysis is detailed in Methods. Peaks overlapping with promoter regions
255 are highlighted in blue, while those overlapping with intergenic regions are highlighted in yellow.
256 The promoters of the 11 hematopoietic transcription factors are indicated. Only 3 of them
257 (RUNX1, CBFA2T3, TAL1) showed significant differential changes in accessibility between 0h
258 and 5h. After 5h, none of the TF showed significant changes in their TSS region. Note that a TF
259 can be displayed more than once, it is explained by the fact that a TF can have multiple TSSs, also,
260 more than one peak can fit the TSS region.
261
262 We explored further the chromatin dynamics in promoter regions of 11 TF-encoding genes known
263 to act as early hematopoiesis regulators [2]. With the exception of GATA1, every gene has
264 accessible promoters with at least one ATAC-seq peak (**Fig. 5** and **Additional Fig. 3)**, suggesting
265 that even before cell stimulation with cytokines, the promoter regions of these key regulators genes
266 are fully accessible and remain so along the entire experiment.
267
268 To further investigate the gene promoter accessibility, we analyzed the enrichment of various
269 transcription factors binding site (TFBS) motifs among peaks. We observed that many of the TFSs
270 of factors known to play a role in hematopoiesis, such as RUNX1, ERG, PU.1 and FLi1 are already
271 highly accessible at 0h and remain detectable at relatively the same level up to 48h (**Additional**
272 **Fig. 4**). We also note that CTCF (CCCTC-binding factor) binding sites were detected more than
273 five times more frequently among the detected peaks than in other regions, suggesting the
274 implication of chromatin remodeling during this period [15].
275

276 ## Combined scRNA-seq and ATAC-seq Analysis

277

278 In order to elucidate how the dynamics of chromatin accessibility and the differential gene
279 expressions were related, we combined the scRNA-seq and the ATAC-seq data (see Methods). A
280 careful comparison of scRNA-seq and ATAC-seq analysis in **Fig. 1** and **Fig. 5** shows that the
281 wave of opening and closing of accessible gene promoters/transcription start sites (TSSs) precedes
282 the wave of the increase and decrease of the gene transcription. To make sense of this, first we
283 examined how promoter accessibility of the genes is related to the gene expression. Specifically,
284 we grouped the promoters based on the configuration change of ATAC-seq peaks between 5h
285 and 24h (**Fig. 6A**). By doing so, there are 4 possible combinations of chromatin accessibility state:
286 "open-open", "open-close", "close-close" and "close-open", depending on the presence or
287 absence of ATAC-seq peaks at the given promoter at 5h and 24h, respectively. The period between
288 5h and 24h is particularly interesting and important, because most of the changes in gene
289 expression and DNA accessibility occur at this stage. We then identified the target genes for each
290 promoter using the Regulatory Circuit resource (see Methods). Note that a promoter may regulate
291 multiple genes and a gene may be regulated by several promoters. Therefore, the total numbers of
292 promoters and genes may be different. Finally, we examined the overrepresentation of DE and
293 non-DE genes among the groups of genes that are the target of each of the four classes of
294 promoter configuration (i.e. open-open, open-close, close-open, and close-close). The analysis
295 showed a significant overrepresentation (p-value<10e-4) for genes showing DE in the set of genes
296 associated with the "open-open" promoter configuration (**Fig. 6A**). In the "open-close" promoter
297 class, genes showing no DE were overrepresented (**Fig. 6A**). Non-DE genes were also
298 overrepresented in the "close-close" promoter class.

299

300 To understand how alterations in DNA accessibility and TF expressions in combination regulated
301 target gene transcription, we classified genes according to whether any of the TFs were
302 differentially expressed between two different time points, 5h and 24h, as we had done earlier –
303 that is, "changes in TF" vs. "no change in TF" grouping (details about the method are explained
304 in **Additional Fig. 5**). We tested the overrepresentation of DE genes among the eight groups of
305 genes based on the different classes of promoter configuration and the DE of the TFs (**Fig. 6B**).
306 We found a significant overrepresentation for DE genes among the genes with at least one of the
307 TFs differentially expressed, but only when the target promoters were accessible at both time
308 points, i.e. in the "open-open" configuration. For the same "open-open" promoter configuration,
309 genes with no change in expression between 5h and 24h were significantly overrepresented in the
310 gene set whose TF expressions were not altered. In other terms, the regulatory action of the TFs
311 can only be observed if and only if the promoters of the target genes are already accessible and
312 remain so between the two time points.
313
314 Similar analysis was done between 24h and 48h (**Additional Fig. 6**). During this period, promoters
315 that remain accessible are enriched for DE genes, while inaccessible promoters are enriched for
316 genes showing no DE. Interestingly, the combined enrichment analysis of ATAC-seq and scRNA-
317 seq did not show any significant over-representation for DE or non-DE genes.
318
319 Taken together, the integration of gene expression and chromatin accessibility data support the
320 idea that differential expression of genes can be explained by changes in the expression of at least
321 one its TFs. However, the regulatory action of TFs only applies when the promoter remains
322 accessible. Subsequently, the closing of the chromatin on the promoters seems to prohibit the
323 action of TFs.

In order to verify if the observations above hold for specific genes, we compared the gene expression and ATAC-seq profiles of the 11 genes essential for hematopoietic differentiation already considered above (**Additional Fig. 3**) [2]. We saw no correlation between promoter accessibility and transcription. For example, the promoter of the SMAD6 gene is accessible at all time points, still not expressed as shown on the heat-map (**Additional Fig. 2**).

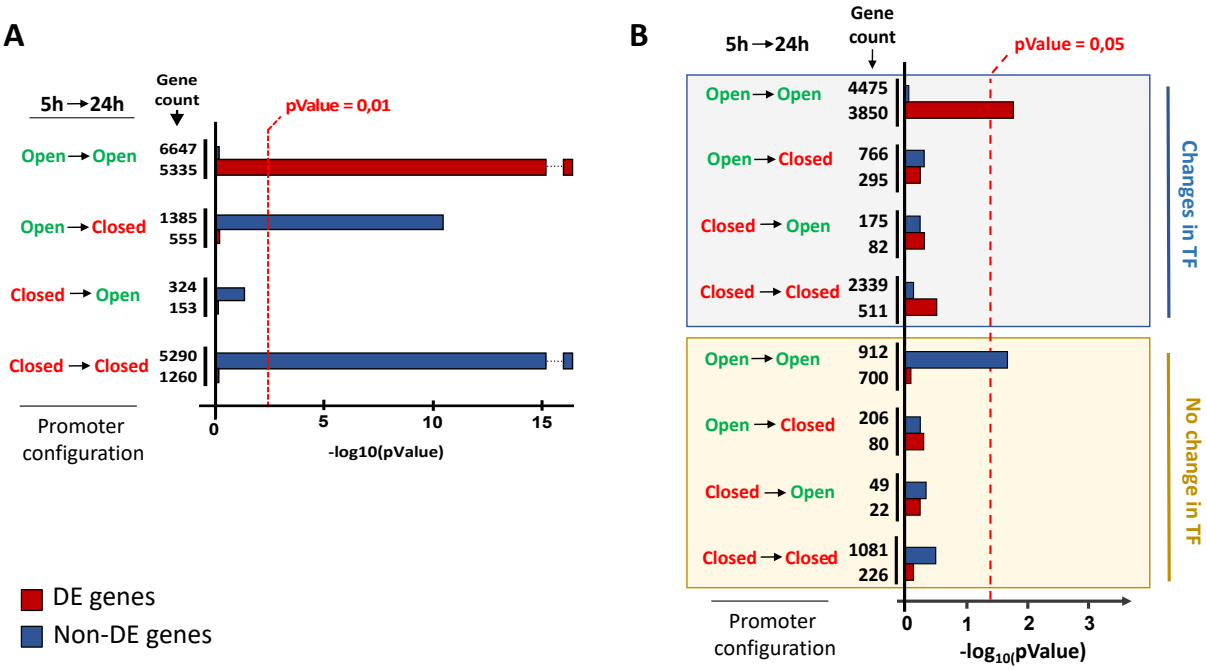

Fig. 6 Promoter configuration dynamics and transcription influence on gene expression regulation between 5h and 24h. A Enrichment analysis for differentially expressed genes (DE) and non-DE genes depending on the promoter accessibility dynamics. **B** Enrichment analysis differentially expressed genes (DE) and non-DE genes depending on the promoter accessibility dynamics and the changes of the expression of TF-encoding genes that regulate them (two-tailed Fisher exact test, see Methods for details).

339 These observations clearly reveal the unequal role of the chromatin configuration and TF action
340 on gene expression and explain the chronology of why the initial increase in DNA accessibility
341 precedes the burst in the level and diversity of gene transcription. Since TF action alone is unable
342 to make the promoters accessible, the initial opening of the chromatin has to be a global and non-
343 specific event. This explains why only a subset of genes with initially accessible promoters become
344 transcribed during the later stages.
345

346 # Discussion

347

348 *In vitro* cultured human cord blood derived CD34+ cells are usually considered as a
349 heterogenous population of cells. Recent studies demonstrated that this heterogeneity is not the
350 result of the mixture of different cell types, but a population of cells with a wide distribution of
351 gene expression patterns [7] that fluctuate, generating morphological instability [6]. The first
352 morphological and molecular signs of the phenotypic diversification appear at the end of the
353 unusually long first cell cycle that follows cytokine stimulation [6]. During the first cell cycle, each
354 cell displays a rather distinct gene expression pattern but is usually morphologically similar. By 48
355 to 72 hours, one can observe the emergence of two different cellular morphologies and two
356 different characteristic transcription profiles [6]. Such an observation prompted us to investigate
357 the narrow window of time within 48h in more details. The observations reported here reveal the
358 interplay between the dynamic chromatin and gene expression changes.
359

360 Using ATAC-seq, we detected at 0h more than 46000 peaks, about 30% of them in gene promoters
361 (TSSs). The number of detected TSSs increased sharply during the first 5 hours of culture (**Fig.**
362 **4**). At the 5h time point, more than 50% of all TSSs promoters in the genome displayed accessible

363 DNA (**Fig. 4B**). After the rapid initial increase, the number of the peaks started to decrease (**Fig.**
364 **4**). There were approximately 16% less accessible TSSs 48 hours later. The number of open
365 intronic and intergenic genomic regions decreased even more rapidly and fell to 50% of the initial
366 number. The tendency to chromatin closing therefore appears as a general feature. Importantly,
367 the wave of chromatin opening and closing is followed by a wave of transcriptional activity. The
368 variety of the transcribed genes and the number of the mRNA molecules per gene was the lowest
369 at 5h – the first time point tested for scRNA-seq – but both increased sharply at 24h, reached a
370 plateau between 48h and 72h and decreased at 96h (**Fig. 1B** and **Fig. 1C**). The 5h-to-48h period
371 corresponds to the multilineage-primed stage of the CD34+ cells that precedes the emergence of
372 the first signs of characteristic gene expression patterns accompanying differentiation [6]. It is a
373 universal feature of the cells during the initial phases of the fate commitment process to progress
374 through a transitional cell state marked by the rise-then-fall in transcriptional uncertainty and a
375 concomitant rise-and-fall of cell-to-cell variability [12]. As reported here, the gene transcription in
376 the CD34+ cells clearly follows the same pattern. The global increase of transcription is preceded
377 by a widespread and non-specific chromatin opening that makes accessible more than 50% of gene
378 promoters in the genome.
379
380 Importantly, there is a strong stochastic component in the establishment of the multilineage
381 primed expression state, because the number of gene promoters that are accessible exceeds the
382 number of actually transcribed genes in each cell by 3 to 5 times (**Fig. 1B** and **Fig. 4B**). The
383 emergence of coherent transcription profiles from this heterogeneous transitory state is preceded
384 by chromatin rearrangements. A significant fraction of gene promoters (16%) and intergenic sites
385 (46%) in the genome become inaccessible through chromatin closing between 5h and 48h (**Fig.**
386 **4B**). The stabilization of the transcriptome is presumably the consequence of these chromatin

387 changes. Some promoters gradually become repressed by chromatin closing, while others are
388 stabilized in an open chromatin configuration. The role of TFs appears crucial at this stage. Indeed,
389 the transcription of a gene is changed between 5h and 24h if the expression of TF-encoding genes
390 that regulate them also changes. However, changes of the expression of the TF-encoding genes
391 do not lead to alteration of their target gene expression if the promoters are in "closed" chromatin
392 configuration around the TSS (**Fig. 6B**), indicating that TFs alone are not able to efficiently
393 regulate the gene transcription, and the chromatin accessibility is a pre-requisite for TF action.
394 Since the number of the open promoters is high at the beginning of the process, a competition for
395 the available TFs among accessible promoters may explain the transcriptional and phenotypic
396 fluctuations observed during this period [6]. These fluctuations cease when the transcriptome is
397 stabilized [6].
398
399 The proposed scenario of general chromatin destabilization followed by a selective repression of
400 the genes is also supported by the observations showing that the inhibition of chromatin
401 compaction using valproic acid (VPA), a histone deacetylase inhibitor, can maintain the
402 multilineage-primed state with promiscuous transcription profile for a long period [6,8,16]. The
403 removal of VPA allows defined transcriptome profiles to be established [8]. Therefore, chromatin
404 structural changes appear to be causally involved both in the generation of a multilineage-primed
405 state and the stabilization of cell fate choice. In line with this conclusion, a recent study of human
406 fetal hematopoietic cells has also concluded that extensive epigenetic but not transcriptional
407 priming of HSC/MPPs occurs prior to lineage commitment [17].
408
409 It will be of particular importance to investigate the process of transcriptome stabilization and the
410 feedback mechanisms that must certainly accompanied it. In this respect, a dynamic positive

411 feedback loop between permissive chromatin and translational output has been previously
412 reported for embryonic stem- and in CD34+ cells [18]. It is noteworthy that many of the genes
413 with the most variable expression that contribute significantly to the specification of the emerging
414 transcription patterns are ribosomal protein (RP) coding genes (**Additional File. 2**), thus
415 impacting the process of translation [19]. A high degree of RP expression heterogeneity has already
416 been observed in hematopoietic cells, where a small subset of RPs can discriminate cell types
417 belonging to different hematopoietic lineages [20]. Therefore, it is possible that, in addition to the
418 TF and promoter interactions, a feedback action of the translational output may also contribute
419 to the stabilization of the chromatin.
420
421 The observed non-specific chromatin opening and the rise of an equally non-specific gene
422 expression as a first step, followed by a slow relaxation toward a defined gene expression pattern
423 and chromatin stabilization, brings a new perspective to our understanding of how cell fate
424 commitment is initiated. According to the conventional view, a switch-like activation of fate-
425 specifying genes, followed by a cascade of activation of specific downstream targets determines
426 cell fate. This view is not compatible with the observations reported here. The alternative
427 possibility is that the typical expression pattern of a committed cell results from the stabilization
428 of a network of interacting set of select genes through a transitory multilineage-primed state that
429 is characterized by stochastic and highly variable expression profile. The transitory stage emerges
430 as a rapid and non-specific answer to a substantial change in the cell's environment that is
431 analogous to the physiological stress response whose role is to prepare the organism to meet new
432 and unforeseen circumstances [21]. Here, we observed a general and non-specific opening of the
433 chromatin that lifts the transcription repression and permits targeted interactions between TFs and
434 gene promoters and enhancers. Put in another way, the quasi-random activation of genes in a cell

435 under stressful conditions generates a potential of a variety of phenotypic traits in the cell. Some
436 of these traits promote the cell's survival under the new constraints imposed by the evolving
437 microenvironment, and they are selectively stabilized by feedback mechanisms. These mechanisms
438 are not yet identified, but explicit hypotheses have been made [22,23]. Therefore, the process of
439 choice can be viewed as a continuing iterative process of constrained optimization of the cell
440 phenotype over time, a kind of "learning process" that is accomplished by the cell through
441 interactions and cooperation with the surrounding cells and environment. This way to frame the
442 question of fate commitment has been theorized long ago [24–26], and single-cell studies in the
443 recent years have provided more and more experimental support [3,6,12,27,28].
444

445 ## Conclusions

446

447 In the present study we show that chromatin accessibility and gene expression follow different
448 dynamics. Most of the gene promoters become accessible immediately after stimulation of the
449 cells. The non-specific chromatin opening is followed 24 h later by a wave of high and unrestrained
450 gene expression. Each cell has disordered and unique expression profile. However, the DNA
451 accessibility at the gene promoters starts to decrease rapidly. It is followed by the decrease of gene
452 expression and the slow emergence of two distinct profiles by the end of the period. This is likely
453 to be the result of a selective repression process because the evolution of the gene expression
454 profile goes from the general toward more specific. This corresponds to the gradual acquisition of
455 two different morphological forms in the cell population.
456

457 # Methods

458

459 ## Cell culture

460

461 Umbilical cord blood from anonymous healthy donors was obtained from Centre Hospitalier Sud
462 Francilien, Evry, France or from Etablissement Français du Sang (EFS), Saint Louis Hospital,
463 Paris, France. Mononuclear cells were isolated from cord blood fractions by density centrifugation
464 using Ficoll (Biocoll, Merck Millipore). Human CD34+ cells were then enriched in the sample by
465 immunomagnetic beads using an AutoMACSpro (Miltenyi Biotec). After collection, enriched
466 CD34+ cells were frozen in a cryopreservation medium containing 90% of fetal bovine serum
467 (Eurobio) and 10% of dimethylsulfoxide (Sigma) and stored in liquid nitrogen.

468

469 After thawing, the CD34+ cells were cultured in a 96-well plate in a humidified 5% CO2 incubator
470 at 37°C. Cells were cultured in prestimulation medium made of X-Vivo (Lonza) supplemented
471 with penicillin/streptomycin (respectively 100U/mL and 100ug/mL - Gibco, Thermo Scientific),
472 50 ng/ml h-FLT3, 25 ng/ml h-SCF, 25 ng/ml h-TPO, 10 ng/ml h-IL3 (Miltenyi) final
473 concentration.

474

475 ## Fast-ATAC-seq

476

477 We used Fast ATAC-seq with minor modifications. This protocol was optimized for blood cells
478 [14]. Prior to transposition, cells were marked with 7AAD and dead cells were removed by FACS
479 (Beckman Coulter). Removing dead cells is an important parameter to ensure clear nucleosome
480 patterns and to improve signal to noise ratio. 5000 living cells were used at each time point. A one-
481 step gentle membrane permeabilization and DNA transposition was performed by adding 50ul
482 transposition mixture (25 uL TD buffer 2X, 2,5uL of transposase TDE1 (Illumina), 0,5 uL

483 digitonin 0,1% (Promega) and 22 uL water) to the cell pellets and by incubating at 37°C for 30
484 minutes under agitation. Obtained Transposed DNA were then purified using MinElute PCR
485 Purification Kit (Qiagen) and preamplified using Nextera barcoded primers (Illumina) and
486 NEBNext High-Fidelity 2xPCR Master Mix (New England Biolabs) for 5 cycles. A quantitative
487 PCR amplification was made on 5uL of the sample with SYBR Green to determine the number
488 of additional cycles in order to generate libraries with a minimal number of PCR cycles and to limit
489 PCR bias (according Corces et al [14]). Appropriate number of PCR cycles were applied on the
490 rest of the pre-amplified samples. PCR fragments were purified with MinElute PCR Purification
491 Kit (Qiagen) to get rid of unused primers. A supplemental purification step was performed using
492 Ampure beads kit (Beckman Coulter) to size-select DNA fragments ranging between 100 and 700
493 pb. ATAC-seq libraries were checked for quality using Bioanalyzer (Agilent) prior to sequencing
494 and sequenced in paired-end mode (2x50bp) on the Illumina HiSeq2500 platform.
495

496 **Single-cell RNA sequencing adapted from MARS-seq**

497

498 To perform scRNA-seq, we adapted MARS-seq protocol (Massively parallel single-cell RNA
499 sequencing) [9]. CD34+ cells were stained with 7AAD to only work living cells and cells were
500 isolated by FACS. Individual cells were sorted into 96-well plates containing 4uL of lysis buffer
501 with specific barcoded RT primers (final concentration: 0,2% Triton, 0,4 U/uL RNaseOUT
502 (Thermofisher Scientific), 400nM idx_RT_primers). Idx_RT_primers (see **Table. 1**) contain a T7
503 RNA polymerase promoter for further *in vitro* transcription (IVT), single cell barcodes
504 (**Additional. File. 3**) for subsequent de-multiplexing and unique molecular identifiers (UMIs)
505 allowing correction for amplification biases. After cell sorting, plates were immediately centrifuged
506 and put into dry ice before storage at -80°C preceding the reverse transcription (RT). To open

507 RNA secondary structure, plates containing single cells were incubated at 72°C for 3 minutes and
508 immediately put in ice. 4uL of RT mix were added in each well (final concentration of RT mix:
509 20mM DTT, 2mM dNTP, 2X First stranded buffer, 5 U/uL Superscript III RT enzyme, 10%
510 (W/V) PEG 8000). PEG8000 was added in the RT mix because it has been shown that it can
511 increase the cDNA yield in scRNA sequencing [26]. ERCC RNA spike-in mix (Thermo Scientific)
512 was also added to the solution for further amplification quality filtering (dilution 1/40.10e7). The
513 plate was then put into thermocycler (thermocycler program: 42°C-2min, 50°C-50min, 85°C-5min,
514 4°C hold).
515
516 After first retro-transcription, samples were pooled (see Jaitin et al [9]) and ExonucleaseI digestion
517 was performed, followed by 1,2X AMpure beads purification kit (Beckman Coulter) to keep only
518 retro-transcribed single strand cDNA. Samples were eluted in 17uL of 10mM Tris-HCl, pH=7,5.
519 Second strand cDNA synthesis (SSS) using NEBNext mRNA second strand synthesis module kit
520 was then performed (SSS mix: 2uL 10x SSS buffer, 1uL SSS enzyme; thermocycler program: 16°C-
521 150min, 65°C-20min, 4°C hold). Obtained cDNA was linearly amplified by overnight IVT
522 (HighScribe T7 High Yield RNA synthesis, NEB) at 37°C under T7 promoter. The product was
523 purified with 1,3X Ampure beads and eluted in 10uL of 10mM Tris-HCl, 0,1mM EDTA. 9uL of
524 amplified RNA were then enzymatically fragmented with 1uL of 10x RNA fragmentation reagents
525 (Thermofisher Scientific) in 70°C for 3 min. The fragmentation was stopped with 34uL of STOP
526 mix (1,2uL Stop solution, 26,4uL AMpure beads, 9,8uL TE) and samples were purified. Differing
527 from original MARSseq protocol, the second RT was done with primers (P5N6_XXXX, **Table.**
528 **1**) containing random hexamers and specific barcode (**Additional. File. 3**) to distinguish the
529 different plates (final concentration: 5mM DTT, 500uM dNTP, 10uM P5N6_XXXX, 1X First
530 stranded buffer, 10U/uL Superscript III RT enzyme, 2U/uL RNaseOUT; thermocycler program:

531 25°C 5min, 55°C 20min, 70°C 15min, 4°C hold). cDNA was purified with 1,2x AMpure beads
532 and eluted in 10uL.
533
534 As for ATAC-seq , the appropriate number of PCR cycles was determined using a fraction of the
535 library with SYBR Green based qPCR as described in Zilionis et al [27] (final concentration: 1x
536 Kapa Hifi HotSTart PCR mix, 1x SybrGreen, 0,5uM mix primer P5.Rd1/P7.Rd2 (Table.1);
537 Thermocycler program: 95°C 3min – 40cycles: 98°C 20sec , 57°C 30sec , 72°C 40sec – 72°C 5min,
538 4°C hold). After PCR amplification, libraries were purified with 0,7x AMpure beads. Libraries were
539 checked for quality, using Bioanalyzer HighSensitivity DNA (Agilent) prior to sequencing.
540 Libraries were finally sequenced in paired-end mode (2x50bp) on Illumina HiSeq2500 platform.
541
542 **Table 1: structure of primer sequences used in scRNA-seq.**

Primer name	Sequence (5' to 3')
Idx RT primers	5'-CGATTGAGGCCGGTAATACGACTCACTATAGGGGCGACGTGTG CTCTTCCGATCTXXXXXXNNNNTTTTTTTTTTTTTTTTTTTTTTN3'
P5N6. XXX	5'-CTACACGACGCTCTTCCGATCTXXXXNNNNNN-3'
P5.Rd1	5'-AATGATACGGCGACCACCGAGATCTACACTCTTTCCCTACA CGACGCTCTTCCGATCT-3'
P7.Rd2	5'-CAAGCAGAAGACGGCATACGAGATGTGACTGGAGTTCAGA CGTGTGCTCTTCCGATCT-3'

543 Idx RT primers: TTTTTTTTTTTTTTTTTTTTTTTTTTN = poly-T allowing matching with mRNA poly-A tail,
544 NNNN = 4 bases UMI (randomly generated), XXXXXX = 6 bases cell barcode (**Additional.**
545 **File. 3**). The rest of the sequence consists of a PCR adaptor and a T7 promoter sequence for
546 further IVT amplification. P5N6 XXX: NNNNNN = random hexamer allowing the capture of
547 the fragmented IVT amplified RNA, XXXX = 4 bases "plate barcode" (**Additional. File. 3**). The
548 rest of the sequence consists of a PCR adaptor. P5.Rd1/P7.Rd2 : P5 and P7 Illumina sequencing
549 adaptors.

550

551 # Bioinformatic analysis

552

553 ## Bulk ATAC-seq

554

555 Raw data processing

556

557 Tn5 adapters sequences were first trimmed with the following command:

558 *< cutadapt -q 20 -g "AGATGTGTATAAGAGACAG; max_error_rate=0.1; min_overlap = 10" -A*

559 *"AGATGTGTATAAGAGACAG; max_error_rate = 0.1; min_overlap = 10" --minimum-length 18 --*

560 *times 2 --pair-filter = both >*

561

562 Genome alignment (hg19) was performed using Bowtie2 with the following parameters:

563 *< bowtie2 -x hg19 --no-unal -X 800 >*

564

565 Only Paired-End fragments were kept, considering mapping quality (phred score = 30). Duplicated

566 reads were removed using Picard MarkDuplicates tool. In attempt to not bias the signal recovered

567 after peak calling due to multiple donors, all paired-end files were randomly downsampled to 16M

568 reads (without disrupting pairs of reads) as regard to the smallest number of reads detected in the

569 cohort (Donor 1 – 0h, see **Additional Table. 2**).

570

571 ATAC-seq peaks were then called on those downsampled files using:

572 *< macs2 callpeak -f BAMPE -g hs -B --broad --broad-cutoff 0.1 --keep-dup all >*

573

574 In order to retain only significant accessibility peaks across samples, each list of peaks used in
575 advanced analysis has been defined as the intersection between peaks of the 3 donors tested at the
576 same time point.
577
578 Peak annotation
579
580 Peaks were assigned to genomic regions thanks to a home-made script based on the FindOverlap
581 function from the R package "GenomicRanges" [29]. Genomic elements positions (TSS, exons,
582 introns, CpG islands and CTCF) were retrieved from UCSC database (hg19). Intergenic category
583 was defined as the exclusion of all other defined categories. No priority has been set across the
584 different genomic elements. Therefore, peaks overlapping several genomic features are counted
585 multiple times, resulting in a total number of peaks across elements exceeding the total number of
586 peaks detected at each time point.
587
588 Peak differential analysis
589
590 DEseq2 tool was used to calculate difference in read count between peaks in two consecutive time
591 points [30]. More precisely, the region considered is defined as the interval formed by the union
592 of two overlapping peaks at *t2* and *t1*.
593
594 Motif enrichment
595
596 Peak motif enrichment analysis was conducted with the tool "findMotifsGenome.pl" from the
597 HOMER software tool suite [31]. Background file was generated using an auto-generated list of

598 random regions across the genome (hg19). Motifs were scanned using the total length of our peaks
599 by providing the option <*size given*>.
600
601 **Single-cell RNA-seq (scRNA-seq)**
602
603 Raw data processing
604
605 Cell and plate barcode demultiplexing steps were accomplished under strict selection criteria with
606 the following command:
607 < *cutadapt -q 30 -e 0 -m 30:20 --no-trim --no-indels --pair-filter = any* >
608 Fasta files for both barcodes (cells and time) sequences are given in **Additional File. 3**.
609
610 ERCC mapping was performed using bowtie2 [32] on ERCC known sequences and regular
611 mapping was performed using STAR [33] on the reference genome version hg19 and aligned reads
612 annotated. After quality filtering, reads and UMIs count per gene and ERCC were calculated for
613 expression analysis.
614
615 Cell and gene filtering
616
617 Chromosome Y was removed from the analysis to avoid unwanted effects and only protein coding
618 genes were kept for further analysis. Cells with less than 80 000 total reads were removed, as well
619 as cells with more than 10% of reads corresponding to mitochondrial RNA. To reduce undesired
620 effect due to PCR non-linear amplification, ERCC spikes were used to assess the linearity of
621 amplification. Pearson correlation coefficient was calculated for each cell, and only cells above 0,6

622 were retained. For each cell remaining, genes were defined as detectable if at least two cells
623 contained more than a single UMI (=transcript) and a minimum of 5 reads in total.
624
625 Single-cell clustering and variability analysis
626
627 Clustering analysis was performed with CALISTA (Clustering and Lineage Inference in Single-Cell
628 Transcriptional Analysis), a numerically efficient and highly scalable toolbox for end-to-end
629 analysis of single-cell transcriptomic profiles. This approach includes single-cell mRNA counts in
630 a probabilistic distribution function associated with stochastic gene transcriptional bursts and
631 random technical dropout events. In the data pre-processing, we removed cells with more than
632 95% of zero expression values and we selected the top 200 most informative genes for further
633 analysis. The optimal number of clusters was chosen to be five based on the eigengap plot (see
634 [10] for more details).
635
636 WGCNA
637
638 We applied Weighted Correlation Network Analysis (WGCNA) [34] to mRNA expression data
639 from each donor, to identify modules of genes with similar gene transcriptional dynamics. We
640 excluded genes without any detectable expression in all samples. In implemented WGCNA, we
641 set the soft-thresholding power for a scale-free topology index of 0,9. For each module, we
642 calculated the mean expression of genes by averaging the UMI counts from the two donors.
643
644 Enrichment Analysis
645

646 We obtained a curated collection of TFs to CAGE-defined promoters to gene isoform mapping
647 for a total of 662 human TFs from the Regulatory Circuits resource [13]. In our analysis, we used
648 only TF – Promoter pairs with moderate confidence scores > 0,5. We grouped genes based on
649 whether the relevant TFs demonstrated differential expressions. More specifically, a classification
650 of "changes in TF" was given to any gene in which one of its TFs showed a differential expression.
651 Otherwise, a classification of "no change in TF" was assigned. A Fisher exact test was used to
652 perform over- and under-representation analysis [35].
653

654 **ATAC-seq and scRNA-seq combined analysis (accessibility – expression)**

655

656 Identification of Promoters that have configurational changes

657

658 In an effort to identify promoter regions that are affected (and not affected) by configurational
659 changes of the chromatin, we used the CAGE-defined promoters to gene isoform mapping from
660 the Regulatory Circuits resource [13] to identify the promoters that overlap with the peaks of
661 ATAC-seq and the corresponding target genes (**see Additional Fig. 5B**). For this purpose, we
662 employed the R Bioconductor package "GenomicRanges" [29]. By comparing the peaks
663 overlapping the promoters between two time points (5h – 24 h and 24h – 48h), we grouped
664 promoters into 4 possible chromatin accessibility configurations: "open-open", "open-close",
665 "close-open", and "close-close".
666

667 Differential gene expression of single-cell RNA sequencing

668

669 We computed Z-scores for every gene in each of the two donors between two different time points
670 using the mean and standard deviation of the UMI counts of approximately 100 single cells.
671
672

673
$$Z_{ij}^{t_2-t_1} = \frac{mean\left(UMI_j^{t_2}\right) - mean\left(UMI_j^{t_1}\right)}{\frac{\left(\left(sd\left(UMI_j^{t_2}\right)\right)^2 + \left(sd\left(UMI_j^{t_1}\right)\right)^2\right)^{1/2}}{10}}$$

674

675 $Z_{ij}^{t_2-t_1}$ denotes the Z-score of the expression change of gene *j* in donor *i* between time t_2 and t_1.
676 An average Z-score between the two donors was computed and used to identify the set of
677 differentially expressed genes. We selected a threshold Z-score of 2 and –2 (i.e., two standard
678 deviations of change) to designate upregulated and downregulated genes, respectively. Collectively,
679 they represent the set of differentially expressed genes.
680

681 <u>Enrichment Analysis of Combined ATAC-seq and scRNA-seq</u>
682

683 For the combined ATAC- and scRNA-seq analysis, we grouped genes into 8 possible groups based
684 on the chromatin accessibility configurations (i.e., one of the following four configurations: "open-
685 open", "open-close", "close-open", and "close-close") and whether any one of their TFs showed
686 differential expression (i.e., one of the following two groups: "changes in TF" and "no change in
687 TF") (**see Additional Fig. 5C**). As with the analysis of scRNA-seq data alone, a gene was assigned
688 to the group "changes in TF" when at least one of its TFs showed differential expression;
689 otherwise, the gene was classified as "no change in TF". Note that different isoforms of the same
690 gene can have distinct TSSs that are under the control of different promoters. Thus, a gene might

691 be counted in more than one category in the chromatin accessibility configurations. Consequently,
692 the total sum of the genes in the 8 groups as described above might exceed the total number of
693 genes. A Fisher exact test was used to perform over- and under-representation analysis [35].
694

695 Declarations

696

697 Ethic statement

698

699 Human cord blood (UCB) was collected from placentas and/or umbilical cords obtained from
700 Etablissement Français du Sang (EFS), Saint Louis Hospital, France or from Centre Hospitalier
701 Sud Francilien, Evry, France in accordance with international ethical principles and French
702 national law (bioethics law n°2011-814) under declaration N° DC-201-1655 to the French Ministry
703 of Research and Higher Studies.
704

705 Availability of data and materials

706 Data are available under the NCBI GEO accession number GSE156735.
707

708 Competing interests

709 None
710

711 Funding

This work was supported by EPHE (11REC/BIMO), ANR grant ANR-17CE12-0031-01 «SinCity ».

Author contribution

AP, AM, RP and JFD designed the study.

RP, AM, LR and SC conducted the experiments.

AM, RS, RG and NPG performed CALISTA analysis.

RP, DS, RS and RG analyzed the ATAC-seq data.

RP, AM, LR, SC, RS, RG, NPG, DS, GC, JC and AP analyzed the results and performed statistical analysis.

RP, AM and LR prepared the figures.

AP, RP and LR wrote the paper with the help of their colleagues.

Acknowledgements

The authors are grateful to Olivier Gandrillon, Camille Fourneaux for helpful discussions and Sunil Laxman and Olivier Gandrillon for the critical reading of the manuscript. The authors are also grateful to Sophie Foulon for her help in scRNA sequencing protocol design.

Reference

1. Kawamoto H, Katsura Y. A new paradigm for hematopoietic cell lineages: revision of the classical concept of the myeloid-lymphoid dichotomy. Trends Immunol. Trends Immunol; 2009.

735 p. 193–200.
736 2. Sive JI, Göttgens B. Transcriptional network control of normal and leukaemic haematopoiesis.
737 Exp. Cell Res. Academic Press Inc.; 2014. p. 255–64.
738 3. Hu M, Krause D, Greaves M, Sharkis S, Dexter M, Heyworth C, et al. Multilineage gene
739 expression precedes commitment in the hemopoietic system. Genes Dev. Cold Spring Harbor
740 Laboratory Press; 1997;11:774–85.
741 4. Nimmo RA, May GE, Enver T. Primed and ready: Understanding lineage commitment
742 through single cell analysis. Trends Cell Biol. Elsevier Ltd; 2015. p. 459–67.
743 5. Pina C, Fugazza C, Tipping AJ, Brown J, Soneji S, Teles J, et al. Inferring rules of lineage
744 commitment in haematopoiesis. Nat Cell Biol. Nat Cell Biol; 2012;14:287–94.
745 6. Moussy A, Cosette J, Parmentier R, da Silva C, Corre G, Richard A, et al. Integrated time-lapse
746 and single-cell transcription studies highlight the variable and dynamic nature of human
747 hematopoietic cell fate commitment. PLoS Biol. Public Library of Science; 2017;15.
748 7. Velten L, Haas SF, Raffel S, Blaszkiewicz S, Islam S, Hennig BP, et al. Human haematopoietic
749 stem cell lineage commitment is a continuous process. Nat Cell Biol. Nature Publishing Group;
750 2017;19:271–81.
751 8. Moussy A, Papili Gao N, Corre G, Poletti V, Majdoul S, Fenard D, et al. Constraints on
752 Human CD34+ Cell Fate due to Lentiviral Vectors Can Be Relieved by Valproic Acid. Hum
753 Gene Ther [Internet]. Mary Ann Liebert Inc.; 2019 [cited 2020 Jun 1];30:1023–34. Available
754 from: https://www.liebertpub.com/doi/10.1089/hum.2019.009
755 9. Jaitin DA, Kenigsberg E, Keren-Shaul H, Elefant N, Paul F, Zaretsky I, et al. Massively
756 parallel single-cell RNA-seq for marker-free decomposition of tissues into cell types. Science (80-
757) [Internet]. American Association for the Advancement of Science; 2014 [cited 2020 Aug
758 21];343:776–9. Available from: https://science.sciencemag.org/content/343/6172/776

759 10. Papili Gao N, Hartmann T, Fang T, Gunawan R. CALISTA: Clustering and LINEAGE
760 Inference in Single-Cell Transcriptional Analysis. Front. Bioeng. Biotechnol. Frontiers Media
761 S.A.; 2020. p. 18–18.
762 11. Peccoud J, Ycart B. Markovian modeling of gene-product synthesis. Theor Popul Biol.
763 Academic Press; 1995;48:222–34.
764 12. Gao NP, Gandrillon O, Paldi A, Herbach U, Gunawan R. Universality of cell differentiation
765 trajectories revealed by a reconstruction of transcriptional uncertainty landscapes from single-cell
766 transcriptomic data. bioRxiv [Internet]. Cold Spring Harbor Laboratory; 2020 [cited 2020 Jun
767 1];2020.04.23.056069. Available from:
768 https://www.biorxiv.org/content/10.1101/2020.04.23.056069v1
769 13. Marbach D, Lamparter D, Quon G, Kellis M, Kutalik Z, Bergmann S. Tissue-specific
770 regulatory circuits reveal variable modular perturbations across complex diseases. Nat Methods.
771 Nature Publishing Group; 2016;13:366–70.
772 14. Corces MR, Buenrostro JD, Wu B, Greenside PG, Chan SM, Koenig JL, et al. Lineage-
773 specific and single-cell chromatin accessibility charts human hematopoiesis and leukemia
774 evolution. Nat Genet. Nature Publishing Group; 2016;48:1193–203.
775 15. Ohlsson R, Bartkuhn M, Renkawitz R. CTCF shapes chromatin by multiple mechanisms:
776 The impact of 20 years of CTCF research on understanding the workings of chromatin
777 [Internet]. Chromosoma. Springer; 2010 [cited 2020 Aug 29]. p. 351–60. Available from:
778 /pmc/articles/PMC2910314/?report=abstract
779 16. Chaurasia P, Gajzer DC, Schaniel C, D'Souza S, Hoffman R. Epigenetic reprogramming
780 induces the expansion of cord blood stem cells. J Clin Invest. American Society for Clinical
781 Investigation; 2014;124:2378–95.
782 17. Ranzoni AM, Tangherloni A, Berest I, Riva SG, Myers B, Strzelecka PM, et al. Integrative

783 Single-cell RNA-Seq and ATAC-Seq Analysis of Human Foetal Liver and Bone Marrow
784 Haematopoiesis. bioRxiv. Cold Spring Harbor Laboratory; 2020;2020.05.06.080259.
785 18. Bulut-Karslioglu A, Macrae TA, Oses-Prieto JA, Covarrubias S, Percharde M, Ku G, et al.
786 The Transcriptionally Permissive Chromatin State of Embryonic Stem Cells Is Acutely Tuned to
787 Translational Output. Cell Stem Cell. Cell Press; 2018;22:369-383.e8.
788 19. Guo H. Specialized ribosomes and the control of translation [Internet]. Biochem. Soc. Trans.
789 Portland Press Ltd; 2018 [cited 2020 Aug 29]. p. 855–69. Available from:
790 https://pubmed.ncbi.nlm.nih.gov/29986937/
791 20. Guimaraes JC, Zavolan M. Patterns of ribosomal protein expression specify normal and
792 malignant human cells. Genome Biol [Internet]. BioMed Central Ltd.; 2016 [cited 2020 Jun
793 1];17:236. Available from: http://genomebiology.biomedcentral.com/articles/10.1186/s13059-
794 016-1104-z
795 21. Braun E. The unforeseen challenge: From genotype-to-phenotype in cell populations.
796 Reports Prog Phys [Internet]. Institute of Physics Publishing; 2015 [cited 2020 Aug
797 29];78:036602. Available from: https://iopscience.iop.org/article/10.1088/0034-
798 4885/78/3/036602
799 22. Paldi A. Stochastic gene expression during cell differentiation: Order from disorder?
800 [Internet]. Cell. Mol. Life Sci. Springer; 2003 [cited 2020 Jul 23]. p. 1775–8. Available from:
801 https://link.springer.com/article/10.1007/s00018-003-23147-z
802 23. Páldi A. Random walk across the epigenetic landscape. Phenotypic Switch. Elsevier; 2020. p.
803 53–76.
804 24. Kupiec JJ. A chance-selection model for cell differentiation. Cell Death Differ. England;
805 1996;3:385–90.
806 25. Kupiec JJ. A Darwinian theory for the origin of cellular differentiation. Mol Gen Genet. Mol

807 Gen Genet; 1997;255:201–8.
808 26. Paldi A. What makes the cell differentiate? Prog Biophys Mol Biol. Pergamon; 2012;110:41–
809 3.
810 27. Mojtahedi M, Skupin A, Zhou J, Castaño IG, Leong-Quong RYY, Chang H, et al. Cell Fate
811 Decision as High-Dimensional Critical State Transition. PLOS Biol [Internet]. Public Library of
812 Science; 2016 [cited 2020 Jun 4];14:e2000640. Available from:
813 https://dx.plos.org/10.1371/journal.pbio.2000640
814 28. Richard A, Boullu L, Herbach U, Bonnafoux A, Morin V, Vallin E, et al. Single-Cell-Based
815 Analysis Highlights a Surge in Cell-to-Cell Molecular Variability Preceding Irreversible
816 Commitment in a Differentiation Process. PLoS Biol. Public Library of Science;
817 2016;14:e1002585.
818 29. Lawrence M, Huber W, Pagès H, Aboyoun P, Carlson M, Gentleman R, et al. Software for
819 Computing and Annotating Genomic Ranges. Prlic A, editor. PLoS Comput Biol [Internet].
820 Public Library of Science; 2013 [cited 2020 Jun 1];9:e1003118. Available from:
821 https://dx.plos.org/10.1371/journal.pcbi.1003118
822 30. Love MI, Huber W, Anders S. Moderated estimation of fold change and dispersion for
823 RNA-seq data with DESeq2. Genome Biol [Internet]. BioMed Central Ltd.; 2014 [cited 2020 Jun
824 1];15:550. Available from: http://genomebiology.biomedcentral.com/articles/10.1186/s13059-
825 014-0550-8
826 31. Heinz S, Benner C, Spann N, Bertolino E, Lin YC, Laslo P, et al. Simple Combinations of
827 Lineage-Determining Transcription Factors Prime cis-Regulatory Elements Required for
828 Macrophage and B Cell Identities. Mol Cell. Mol Cell; 2010;38:576–89.
829 32. Langmead B, Salzberg SL. Fast gapped-read alignment with Bowtie 2. Nat Methods. NIH
830 Public Access; 2012;9:357–9.

831 33. STAR: ultrafast universal RNA-seq aligner [Internet]. [cited 2020 Jun 1]. Available from:
832 https://www.ncbi.nlm.nih.gov/pmc/articles/PMC3530905/
833 34. Langfelder P, Horvath S. WGCNA: An R package for weighted correlation network analysis.
834 BMC Bioinformatics [Internet]. BioMed Central; 2008 [cited 2020 Jun 1];9:559. Available from:
835 https://bmcbioinformatics.biomedcentral.com/articles/10.1186/1471-2105-9-559
836 35. Agresti A. An Introduction to Categorical Data Analysis Second Edition.
837

Supplementary information

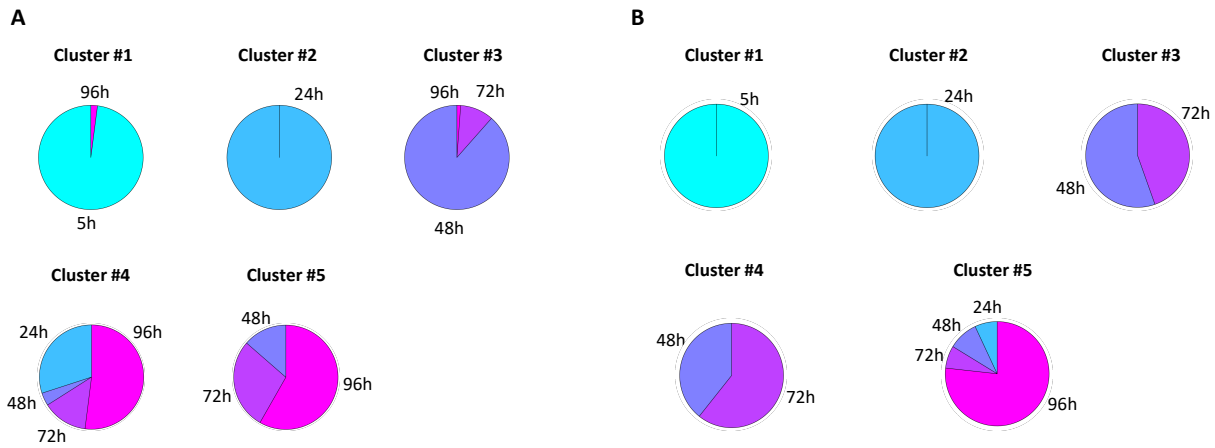

Additional Fig. 1 Repartition of single cells in CALISTA clusters according time of sampling. For each donor, 5 pie charts represent the proportion of cell corresponding to different time points (5h, 24h, 48h, 72h, 96h) defining the 5 clusters computed by CALISTA (**Fig. 2)**. Note that cluster #1 and cluster #2 are almost uniformly composed of cells from 5h and 24h respectively. Starting from 48h, cells tend to fall into several clusters, indicating multiple routes. At 96h, corresponding to the lowest transcriptional level measured, we can observe that cells start to resemble each other again. **Left panel:** Donor 1, **right panel:** Donor 2.

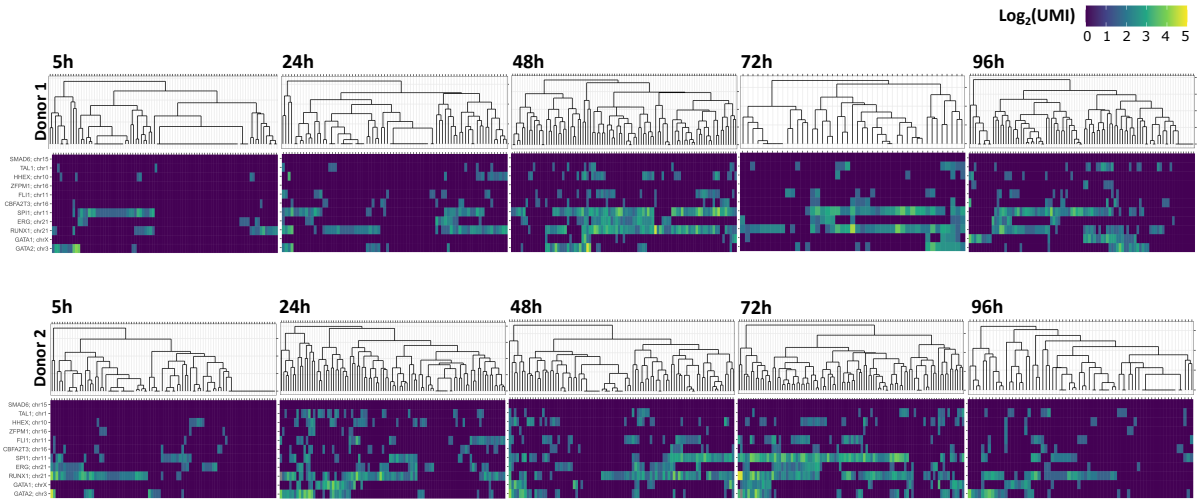

Additional Fig. 2 Heat-map of 11 TFs known to play a role in hematopoiesis regulatory network. For each donor, 5 heat maps (one per time point) were drawn on the basis of gene expression intensity for the 11 TFs described in [13]. Gene expression was measured as the sum of UMIs for each gene considered, a log2 transformation was applied for better visualization. Note that for the gene SMAD6, no transcripts were detected, all time and donor considered.

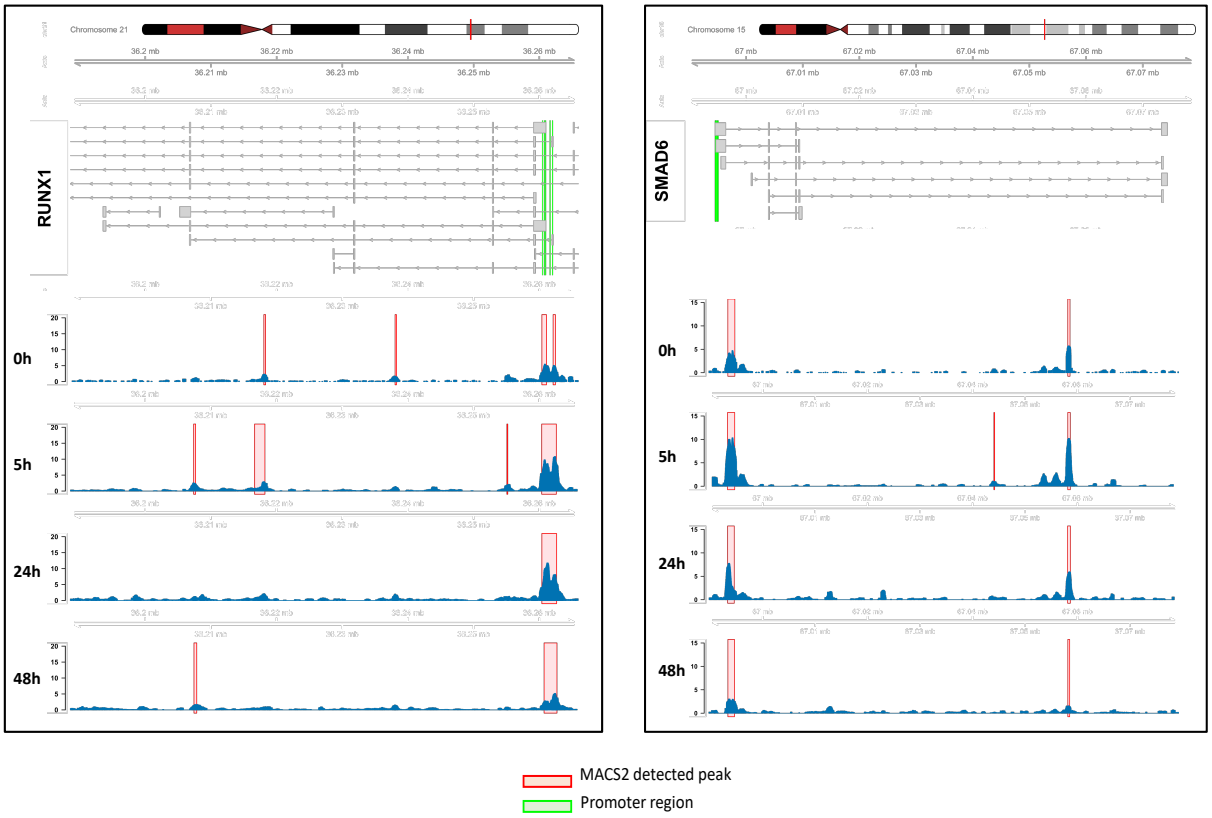

Additional Fig. 3 Detailed accessibility profiles of 2 TFs known to play a role in hematopoiesis regulatory network. For the sake of clarity, only two out of the 11 TFs described in [2] are represented here. The rest of the coverage plots can be found in **Additional File.4**. Green regions drawn on gene sequence represent CAGE-defined promoter considered in this study [13]. Red regions represent peaks computed with MACS2 algorithm. Blue "signal" depicts read coverage for one of the three samples available for each time point (the most representative one). Note that except for GATA1, promoter regions always overlap with detected peaks, no matter the time considered. Interestingly, whereas SMAD6 promoter is accessible, no transcript was detected for both Donor 1 and Donor 2, all times considered (**Additional Fig. 2**). This illustrates that accessibility is not sufficient to guarantee transcription.

		p-value				% of detection in peaks				% of detection in random background			
		0h	5h	24h	48h	0h	5h	24h	48h	0h	5h	24h	48h
CTCF		1e-2126	1e-2418	1e-1180	1e-838	13.10%	15.75%	12.62%	12.60%	2.58%	3.62%	3.69%	3.86%
Fli1		1e-1907	1e-1705	1e-1440	1e-927	46.77%	52.81%	52.66%	52.05%	25.77%	32.94%	32.56%	33.46%
SPi1		1e-1615	1e-1427	1e-1427	1e-637	23.94%	27.60%	26.33%	23.90%	9.68%	13.40%	12.48%	12.37%
ERG		1e-1654	1e-1375	1e-1169	1e-667	53.49%	60.78%	59.28%	56.41%	33.04%	42.51%	40.75%	40.33%
RUNX1		1e-697	1e-452	1e-525	1e-327	29.49%	34.28%	32.64%	30.48%	18.26%	24.87%	21.81%	20.83%

Additional Fig. 4 Motif enrichment for selected known hematopoiesis related transcription factors. At each time point, peak sequences were scanned by HOMER for significantly enriched "known motifs". The motifs selected here illustrate a significant enrichment (zero or one occurrence per sequence coupled with the hypergeometric enrichment calculations) of motifs associated with hematopoiesis and chromatin remodeling. For an extensive list of tested motifs, see **Additional File.5**.

38

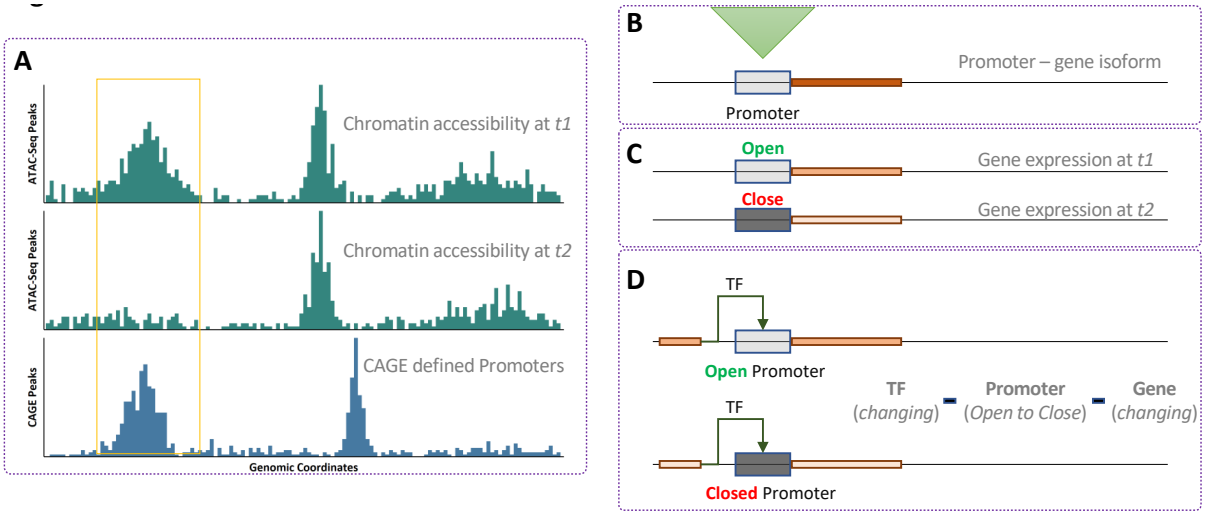

39

40 **Additional Fig. 5 Combined Analysis of scRNA-seq Single cell RNA expression with**
41 **ATAC-seq chromatin accessibility peaks. A** An example showing the changes in the
42 configuration of the chromatin reflected by differences in the peaks of the ATAC-seq and aligning
43 the genomic coordinates with CAGE-defined promoter region (yellow box). **B** The CAGE-
44 defined promoters are linked to gene isoforms. **C** Changes in the promoter accessibility from the
45 ATAC-seq is integrated with the changes in the expression of the gene (RNA-Sequencing of single-
46 cells). In this example, the promoter changes from an open configuration to a close configuration,
47 and the gene isoform in its control changes expression. **D** TFs are then linked to the promoter
48 using moderate to high confidence of motif occurrences in the specific genomic region. TFs
49 themselves could change in their expression. In the example shown, the TF changes in expression,
50 subsequently acting on a promoter that changes from an open to a close configuration and finally
51 regulating a gene that changes in its expression between time *t2* and *t1*.

52

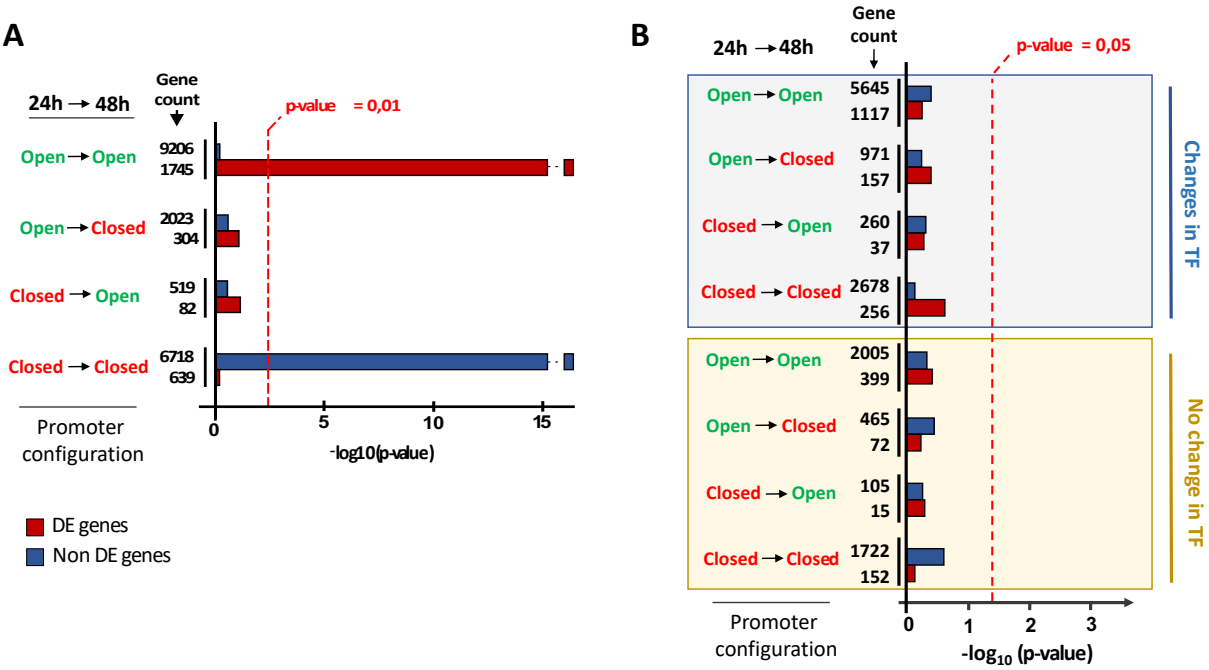

Additional Fig. 6 Promoter configuration dynamics and transcription influence on gene expression regulation between 24h and 48h. A Enrichment analysis for differentially expressed genes (DE) and non-DE genes depending on the promoter accessibility dynamics. **B** Enrichment analysis differentially expressed genes (DE) and non-DE genes depending on the promoter accessibility dynamics and the changes of the expression of TF-encoding genes that regulate them.

Additional Table. 1. Impact of quality filters on the number of cells retained for final analysis.

			Quality filters		
Time	**Donor**	**Initial**	**UMI sum filter**	**Chr Mito filter**	**ERCC spike filter**
5h	1	96	88	88	88
24h	1	96	79	78	78
48h	1	96	93	93	93
72h	1	96	45	45	45

96h	1	96	89	89	89
5h	2	96	88	88	88
24h	2	96	95	95	95
48h	2	96	92	91	88
72h	2	96	96	96	94
96h	2	96	72	70	68

Initially, we lysed 96 cells for each condition. First, we filtered out cells with less than 80 000 reads in total. Among remaining cells, cells with more than 10% of reads assigned to mitochondrial genome were also not included in the final dataset. Finally, ERCC spikes allowed removing cells with not satisfying linear amplification criterion (Pearson coefficient < 0,6).

Additional Table. 2 Total number of peaks in ATAC-seq samples and number of common peaks retained for analysis.

	0h			5h			24h			48h		
	Donor 1	Donor 2	Donor 3	Donor 1	Donor 2	Donor 3	Donor 1	Donor 2	Donor 3	Donor 1	Donor 2	Donor 3
Unique pairs of reads detected	8 391 299	14 310 319	15 701 894	13 372 383	17 359 415	14 998 407	16 460 386	19 605 272	11 588 529	8 569 939	14 513 711	12 665 206
Nb peaks detected after down sampling	66 155	72 075	66 708	60 734	78 486	68 173	54 288	70 713	65 096	50 404	55 249	49 219
Nb common peaks between donors	46 942			47 023			38 711			29 255		

We randomly downsampled each sample to the same level of 16M reads. Peak calling was applied on downsampled bam files. Finally, we considered only the intersection of the 3 peaks dataset available at each time point for further analyses.

Additional File. 1 GO terms results for scRNA-seq WGCNA clusters

74 **(GO_results_WGCNA_clusters.xlsx).**

75

76 **Additional File. 2 CALISTA 200 most variable genes matrix and cluster transition genes**

77 **(CALISTA_200_Top_Variable_Genes.xlsx).**

78

79 **Additional File. 3 scRNA-seq barcode sequences used for cell and plate demultiplexing**

80 **(scRNA-seq_barcodes.tar.gz).**

81

82 **Additional File. 4 Detailed accessibility profile of 11 TFs known to play a role in**

83 **hematopoiesis regulatory network (11_TF_Gene_Coverage.tar.gz).**

84

85 **Additional File. 5 Motif enrichment obtained with HOMER for 400 known motifs between**

86 **t = 0h and t = 48h (homer_results.tar.gz).**

87